

# The Lensing Galaxy in MG1549+3047

*Submitted to AJ: 1995.09.22, revised: 1995.11.20, accepted: 1996.01.17.*

J. Lehár<sup>1</sup>, A.J. Cooke<sup>2</sup>

Institute of Astronomy, Cambridge University, CB3 0HA, UK

C.R. Lawrence

Jet Propulsion Laboratory 169-506, Pasadena, CA 91109

A.D. Silber

Univ. of Washington, Dept of Astronomy FM-20, Seattle, WA 98195

and

G.I. Langston

National Radio Astronomy Observatory, Green Bank, WV 24944

## ABSTRACT

We have measured a velocity dispersion for the foreground galaxy in this gravitationally lensed system. Our dispersion confirms the prediction from lens models, provided that the source is distant enough ( $z_s > 0.2$ ). Current interpretations of lensing statistics depend sensitively on how the optical and mass dispersions are related. For  $z_s > 0.5$ , our observations favor  $\sigma_{mass}/\sigma_{opt} \simeq 1$ , but our uncertainties prevent us from clearly distinguishing between dynamical models. We could not obtain a unique mass profile from lensing constraints, but models with a constant mass-to-light ratio are possible. We also found unusual rotation in the lensing galaxy, and confirmed its redshift.

*Subject headings:* Gravitational Lenses — Dark Matter —  
Radio Sources: individual (MG1549+3047)

---

<sup>1</sup>Present Address: Center for Astrophysics, 60 Garden St, Cambridge, MA 02138, jlehar@cfa.harvard.edu

<sup>2</sup>Present Address: Institute for Astronomy, Royal Observatory, Edinburgh, UK

## 1. Introduction

Early examples of gravitational lensing (e.g., Walsh *et al.* 1979) consisted of several compact images of quasars. When the background source is extended (e.g., Hewitt *et al.* 1988), the images can join in a ring of emission around the lensing galaxy, and multiply-imaged source features can provide many constraints on the lensing mass distribution. For MG1549+3047, the background source is an extended radio lobe (Lehár *et al.* 1993), whose unusual structure is easily explained by a simple lensing model. Here we will be mostly concerned with the lensing galaxy, G1 (see Fig. 1 in Lehár *et al.* 1993), which lies directly in front of the Northwest radio lobe.

Assuming an isothermal mass profile for G1, Lehár *et al.* (1993) predicted its central velocity dispersion to be  $\sigma_{mass} \sim 230 \text{ km s}^{-1}$ . A measured optical velocity dispersion  $\sigma_{opt}$  should be comparable to this value. Of course, neither the mass nor the stellar profiles need be isothermal. For a Hubble profile stellar population in an isothermal gravitational potential,  $\sigma_{mass}/\sigma_{opt} = \sqrt{3/2}$  (Gott 1977). This factor strongly affects the interpretation of lensing statistics (e.g., Turner *et al.* 1984). However, considering a wider range of dynamical models, and taking observational limitations into account, Kochanek (1993) expects that  $\sigma_{mass}/\sigma_{opt} \simeq 1$  in most cases. Systems like MG1549+3047 provide a rare opportunity to test this prediction, since gravitational lensing can probe the total mass distribution.

## 2. Observations

We obtained long slit spectra of G1 on the night of 1992.04.28 at the 4.2 m William Herschel Telescope, using the red arm of the ISIS spectrograph. An EEV CCD detector was illuminated via the R600R grating, centered on 5750 Å, with a 5300 Å dichroic. This arrangement gave 0.73 Å per pixel, or 38 km s<sup>-1</sup>, and a spectral coverage of 5320 – 6180 Å. The slit width was 1" on the sky ( $\sim 3$  pixels or 114 km s<sup>-1</sup>), and was aligned with the major axis of G1 (PA = -151°). The field of view along the slit was  $\sim 1'$ . Six 30-minute exposures were taken. Using the same instrument configuration on 1992.05.01, we observed one radial velocity standard star of spectral type K2 (K2.1=HD155642), and two of type K5 (K5.1=HD155581, K5.2=HD156649). The spectra were reduced using standard IRAF procedures, and re-sampled into 44.6 km s<sup>-1</sup> bins. Figure 1 shows the sum of all six G1 spectra (G1.sum), along with a standard star spectrum.

We measured the velocity dispersion in G1 using a standard cross-correlation method (Tonry & Davis 1979; IRAF task "fxcor"). The three radial velocity standard star spectra

were used as templates. We removed 5th order spline fit baselines from the spectra and apodized by a 10% cosine bell, before Fourier transforming and applying a high-pass filter of  $\sim 10$  in wavenumber. Finally, we fitted a Gaussian to the maximum correlation peak to determine its width and offset. We calibrated the correlation peak width using synthetic galaxy spectra (the template star spectra convolved with known Gaussian dispersions, see Figure 2). The results are summarized in Table 1. The K2.1 template gave higher cross-correlations than the K5 stars, so it is probably a better model of the G1 absorption features. We estimated the “random” contribution to the measurement uncertainty by performing separate cross-correlations for each of the six G1 exposures, and taking the rms of the dispersions. The “systematic” uncertainty, due to template mismatch, was estimated from the range of dispersions obtained when different stellar templates were used. Combining these estimates in quadrature, we found  $\sigma_{opt} = 227 \pm 18 \text{ km s}^{-1}$ .

Our cross-correlation analysis also yields a radial velocity of  $cz = 33534 \pm 103 \text{ km s}^{-1}$  for G1. This result confirms a previously reported redshift of 0.111 (Paturel *et al.* 1989).

Since G1 is extended, we extracted spectra for seven  $1.^{\prime\prime}7$  apertures parallel to the galaxy trace in the co-added data. The cross-correlation results are given in Table 1, and Figure 3 shows the velocity profiles. The radial velocity shows a strong linear trend, which indicates that G1 is rotating.

### 3. Discussion

Our velocity dispersion,  $\sigma_{opt} = 227 \pm 18 \text{ km s}^{-1}$ , is very close to the  $\sigma_{mass}$  derived for an isothermal lens model (Lehár *et al.* 1993). The two mass estimates remain comparable for any source redshift  $z_s > 0.2$ , confirming the basic lensing prediction. The radio properties and optical color of the source suggest that  $z_s > 0.3$  (Lehár *et al.* 1993). Furthermore, MG1549+3047 is a steep spectrum source drawn from a flux-limited radio source list (Lehár 1991). Assuming a spectral index of  $-1$ , the selection cutoff corresponds to the flux limit of the Parkes 2.7 GHz radio survey (Dunlop & Peacock 1990), for which  $\langle z \rangle \sim 0.7$  has been measured. Thus  $z_s > 0.5$  is most likely.

The systematic shift in radial velocity implies that G1 is rotating. The velocity is still increasing in the outermost apertures, so the maximum  $v_{max}$  must exceed  $200 \text{ km s}^{-1}$ . G1 can be compared to an oblate isotropic rotator using the  $(v_{max}/\sigma)^*$  factor (Kormendy 1982), which exceeds 2. From its color and radial profile, G1 appears to be an early-type galaxy (Lehár *et al.* 1993). Most ellipticals rotate more slowly, and this level of rotation is more characteristic of S0 galaxies or the bulges in disk galaxies (Davies *et al.* 1983).

The optical velocity dispersion can be compared with the total mass dispersion from lens models. Assuming a source redshift of  $z_s = 1$ , the lens model gives an isothermal velocity dispersion  $\sigma_{mass} = 230 \pm 11 \text{ km s}^{-1}$  (Lehár *et al.* 1993), which is the same as  $\sigma_{opt}$ . If the stellar tracers are assumed to have a Hubble profile, the expected optical dispersion will be  $188 \pm 9 \text{ km s}^{-1}$  (Gott 1977); and the strong rotation in G1 does not affect this. Our  $\sigma_{opt}$  differs from this prediction by almost two standard deviations, and agrees with the expectation of Kochanek (1993). However,  $\sigma_{mass}$  increases by 25% if the source redshift  $z_s = 0.3$ . So although our observation favors  $\sigma_{mass}/\sigma_{opt} \simeq 1$ , we cannot clearly distinguish between the two dynamical models.

We can also probe the dark matter distribution by comparing the lens models with the optical surface brightness profile. Using the IRAF task “ellipse”, we extracted profiles from each of the CCD images reported in Lehár *et al.* (1993). Figure 4 shows the average profile for the  $I$  filter exposures. For sky surface brightnesses  $\Sigma(\theta)$ , we used a model of the form:

$$\Sigma(\theta) = \Sigma_0 \left[ 1 + \left( \frac{\theta}{\theta_c} \right)^2 \right]^{-P/2} ,$$

where  $P = 1$  corresponds to an isothermal distribution, and  $P = 2$  yields a Hubble profile. We found best fit models for each of the observed profiles, varying  $\Sigma_0$ ,  $\theta_c$ , and  $P$ . The best fit shape parameters,  $\theta_c = 0.24 \pm 0.05$  and  $P = 1.94 \pm 0.05$ , did not vary with color. Here, the uncertainties are the rms of the parameter values, obtained from separate fits to each profile. For the mass distribution, we used a surface density model of the same form, with a quadrupole perturbation to account for the ellipticity  $\epsilon = (1 - b/a)$  (Miralda-Escudé 1993). The same image constraints and search method were applied as in Lehár *et al.* (1993). There is a strong correlation between  $\theta_c$ ,  $\epsilon$  and  $P$  (see Figure 5). The  $\chi^2$  values are very small, probably because the position uncertainties in Lehár *et al.* (1993) are overestimated. To estimate the parameter uncertainties, we performed Monte Carlo simulations, where the image positions were perturbed within their assumed  $0''.1$  uncertainties. When  $P$  is close to its optical value, the best fit  $\theta_c$  is also consistent with the optical profile, provided that  $\epsilon \simeq 0.3$ . So although we cannot uniquely determine  $P$ , the lens constraints are consistent with the mass and light distributions being the same.

We are now very close to a fully self-consistent lensing model for this system, and MG1549+3047 is promising for mass distribution studies. The background radio lobe has many structures, and it straddles the multiple-imaging boundary (see Lehár *et al.* 1993). These properties are best exploited by the “Lensclean” method (Kochanek & Narayan 1993), which uses all of the source structure to constrain a lens model. The distance to the source is still unknown, however, and this deficiency affects many model predictions. Obtaining the source redshift remains an important objective.

We thank many people for helpful discussions, in particular Paul Hewett, Jordi Miralda-Escudé, Dave Carter, Chris Kochanek, Emilio Falco, and Hans Rix. IRAF is distributed by NOAO which is operated by AURA Inc. under contract to the NSF. JL gratefully acknowledges support from a PPARC associateship, and from NSF grant AST93-03527.

## REFERENCES

Davies R.L., Efstathiou G., Fall S.M., Illingworth G., Schechter P.L., 1983, *ApJ*, 266, 41

Dunlop J.S., Peacock J.A., 1990, *MNRAS*, 247, 19

Gott J.R.III, 1977, *ARA&A*, 15, 258

Hewitt J.N., Turner E.L., Schneider D.P., Burke B.F., Langston G.I., Lawrence C.R., 1988, *Nature*, 333, 537

Kochanek C.S., 1993, *ApJ*, 419, 30

Kochanek C.S., Narayan R., 1993, *ApJ*, 401, 461

Kormendy J., 1982, in “Morphology and Dynamics of Galaxies”, ed. L. Martinet, M. Mayor, (Sauverny:Geneva Obs.), p. 115

Lehár J., 1991, MIT Ph.D. Thesis

Lehár J., Langston G.I., Silber A., Lawrence C.R., Burke B.F., 1993, *AJ*, 105, 847

Miralda-Escudé J., 1993, *ApJ*, 403, 497

Paturel G., Fouqué P., Bottinelli L., Gouguenheim L., 1989, in “Catalog of Principal Galaxies”, (Lyon:Obs. de Lyon et Paris-Meudon)

Tonry J., Davis M.A.J., 1979, *AJ*, 84, 1511

Turner E.L., Ostriker J.P., Gott J.R.III, 1984, *ApJ*, 284, 1

Walsh D., Carswell R.F., Weymann R.J., 1979, *Nature*, 279, 381

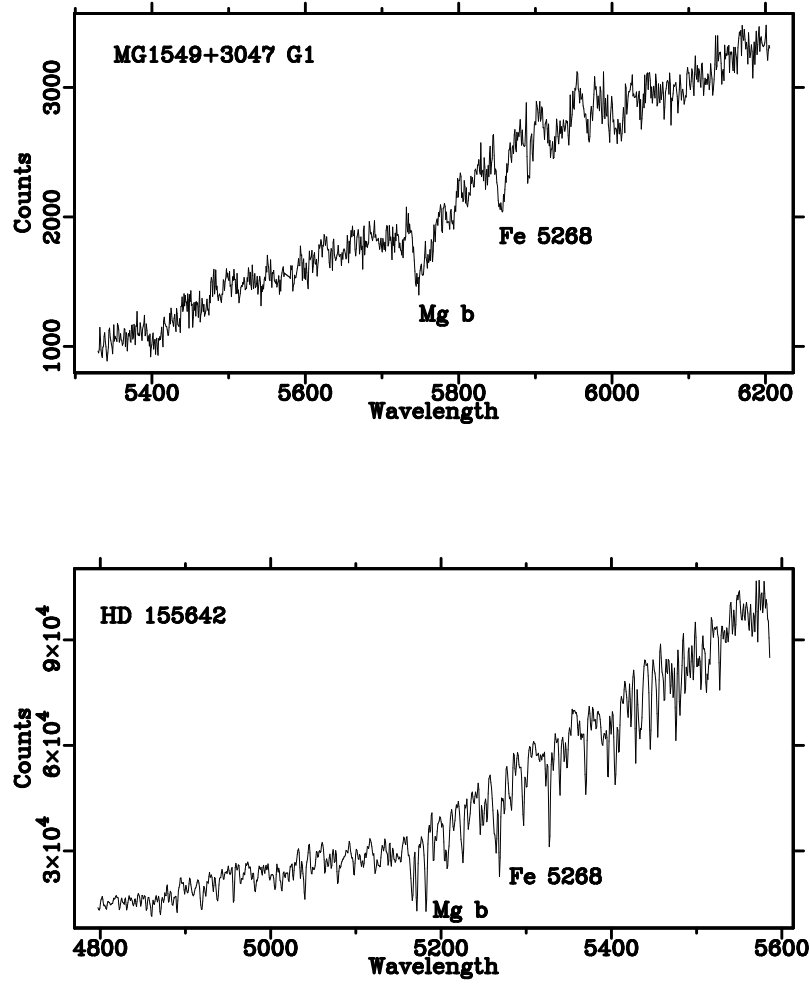


Fig. 1.— Optical spectra for G1 (G1.sum) and a template star HD 155642 (K2.1). The G1 spectrum is the sum from all six exposures. Wavelengths are given in Angstroms, and two major absorption features are labelled.

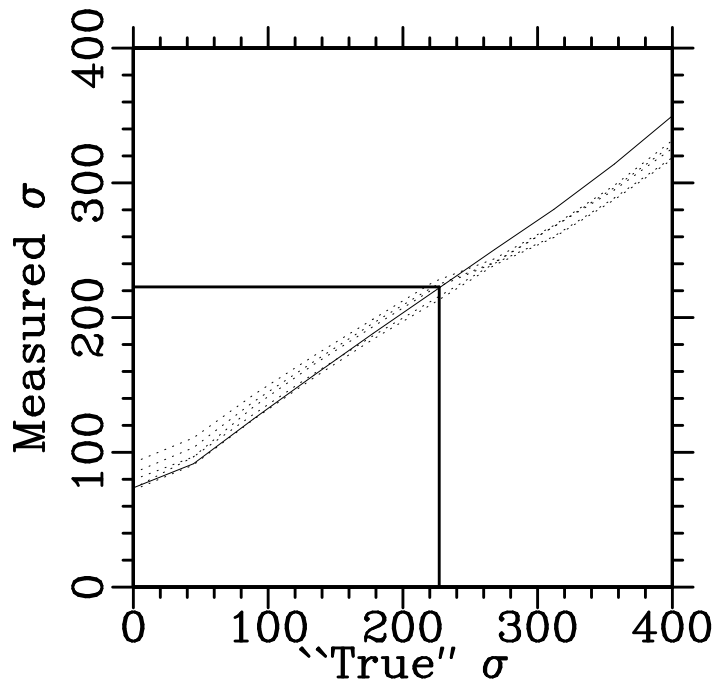


Fig. 2.— Velocity dispersion calibration curve. This shows the velocity dispersion (in  $\text{km s}^{-1}$ ) measured from model spectra with known “true” dispersions. The solid curve shows the result when K2.1 was used for both the model and template spectrum, and the dotted curves show other combinations of model and template. The heavy line shows how the observed G1 correlation width converts to  $\sigma_{opt}$ .

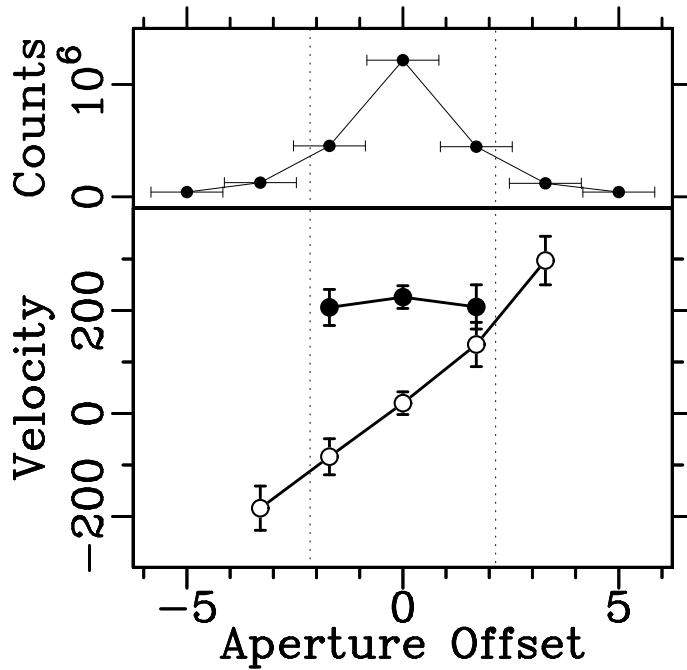


Fig. 3.— Velocity profiles for G1, as a function of aperture position (in arcsec NW of G1). The lower panel shows the radial velocity (open circles) and the velocity dispersion (solid dots), both in  $\text{km s}^{-1}$ . Error bars are the formal uncertainties from “fxcor”. The upper panel shows the total counts in each aperture, and the extent of each aperture is shown as a horizontal bar. The dotted lines in both panels show the original  $4.3''$  aperture.

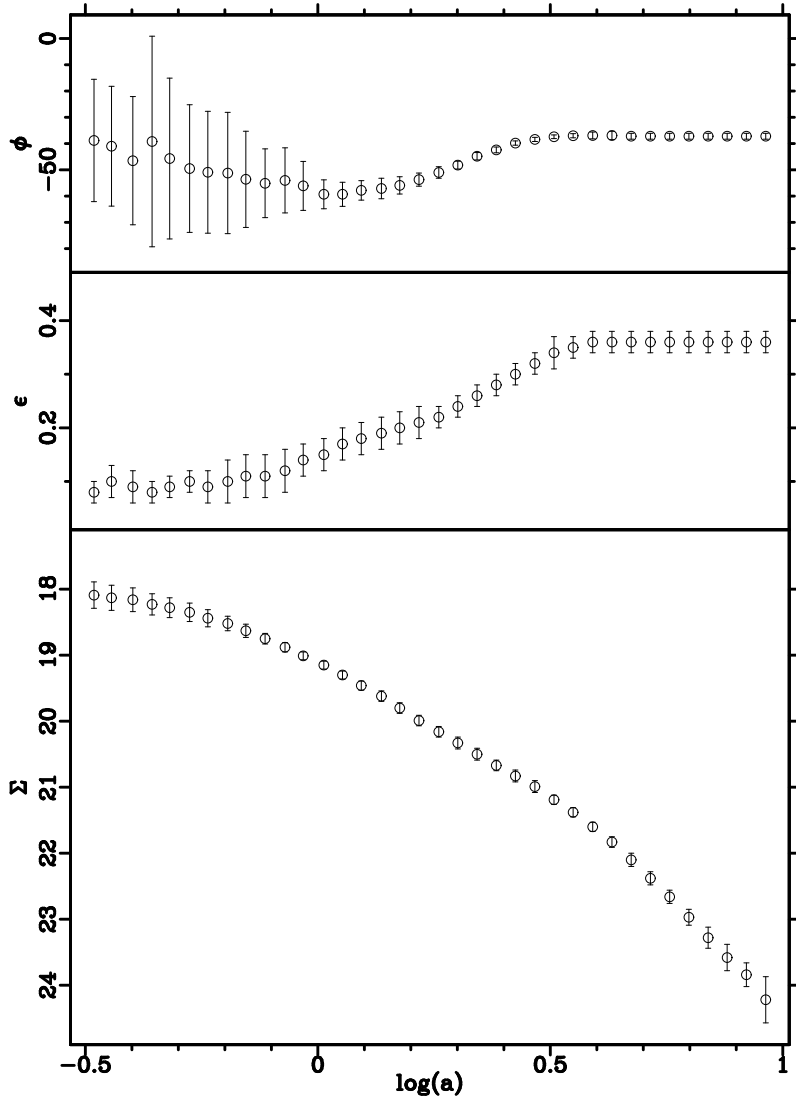


Fig. 4.— Average surface brightness profiles for G1, as a function of semimajor axis  $a$  (in arcsec), from the  $I$  filter CCD observations of Lehár *et al.* (1993). The lower panel shows the surface brightness  $\Sigma$ , in  $\text{mag}/\text{arcsec}^{-2}$ . The middle and upper panels show the ellipticity  $\epsilon = (1 - b/a)$ , and the major axis orientation  $\phi$  (in degrees CCW from North). The error bars indicate the rms between profiles from each of the separate  $I$  filter exposures. Note that both  $\epsilon$  and  $\phi$  vary with radius, and that some of this may be due to atmospheric seeing.

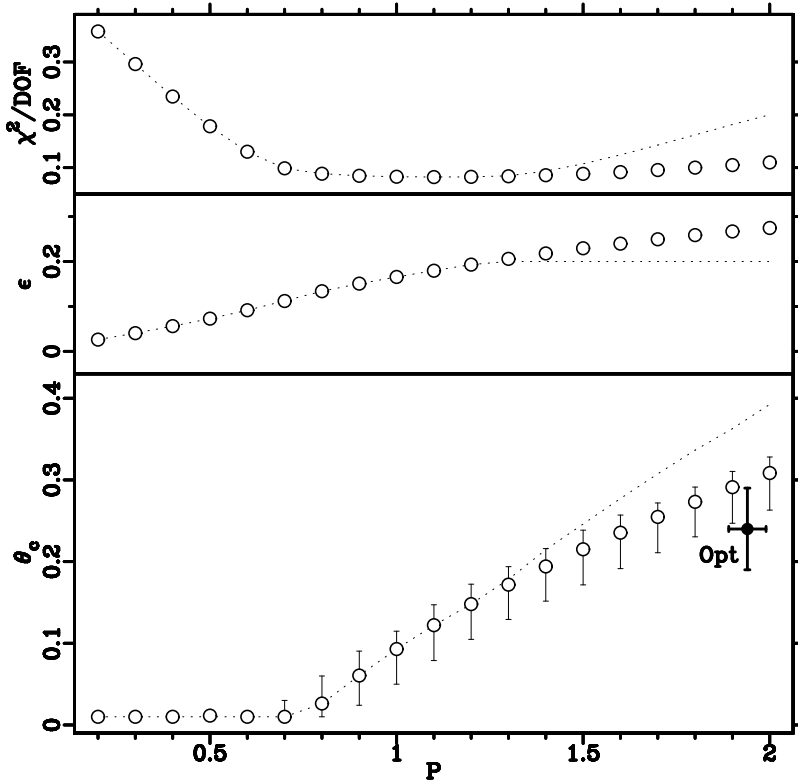


Fig. 5.— Lens model parameters for various values of the mass index  $P$ . The lower panel shows the core radius  $\theta_c$  (in arcsec), with the best fit optical values indicated. The middle panel shows the ellipticity  $\epsilon = (1 - b/a)$ , and the upper panel shows the  $\chi^2$  per degree of freedom. The error bars show the 68% confidence intervals in  $\theta_c$ , from Monte-Carlo simulations (100 for each  $P$ ). The dotted curves show the best fit parameter values if  $\epsilon < 0.2$  is applied as a constraint.

TABLE 1  
SPECTRAL CROSS-CORRELATION RESULTS

Spectrum	Template	Corr.	$r^a$	$cz^b$	$\sigma_{opt}^b$
Summed Spectrum					
G1.sum	K2.1	0.36	17.1	33534	227
G1.sum	K5.1	0.34	14.3	33441	215
G1.sum	K5.2	0.32	13.9	33435	228
Separate Spectra					
G1.1	K2.1	0.25	8.8	33552	200
G1.2	K2.1	0.25	9.4	33527	222
G1.3	K2.1	0.22	6.9	33573	213
G1.4	K2.1	0.27	9.0	33537	239
G1.5	K2.1	0.25	8.7	33486	221
G1.6	K2.1	0.25	8.9	33533	219
Subapertures from Summed CCD Image					
+5''0 NW	K2.1	0.08	2.5	(33806)	
+3''3 NW	K2.1	0.14	4.5	33831	(109)
+1''7 NW	K2.1	0.22	7.9	33668	207
0''0 NW	K2.1	0.35	17.5	33554	226
-1''7 NW	K2.1	0.29	9.9	33450	206
-3''3 NW	K2.1	0.15	4.5	33350	(100)
-5''0 NW	K2.1	0.06	1.8	(33432)	

<sup>a</sup>Tonry & Davis (1979) signal/noise estimator.

<sup>b</sup>Velocity in ( $\text{km s}^{-1}$ )